China Geology 8 (2025) 797−805

China Geology

Journal homepage: http://chinageology.cgs.cn
https://www.sciencedirect.com/journal/china-geology

Lishiite, $(Ca_2□)Sr_3(CO_3)_5$, a new burbankite mineral from carbonatite-syenite complex in Shaxiongdong, Hubei, China

Jie Dai[a, b], Xiao-dong Pan[c,*], Tong Wang[d], Guo-wu Li[e], Guan Wang[a], Shang-ke Xie[a], Jing Ren[a], Kun-yang Wang[a], Ting Li[f], Tao Wang[f], Jia-le He[a], Jin-sha Xu[a], Gan-fu Shen[a]

[a] *Chengdu Center, China Geological Survey(Southwest China Innovation Center for Geosciences), Ministry of Natural Resources, Chengdu* 610218, *China*
[b] *The Key Laboratory of Sedimentary Basin and Oil and Gas Resources, Ministry of Natural Resources, Chengdu* 610218, *China*
[c] *Sichuan Dikun Mining Co., Ltd., Chengdu* 610051, *China*
[d] *Hubei Geological Testing Center, Wuhan* 430034, *China*
[e] *Laboratory of Crystal Structure, China University of Geosciences (Beijing), Beijing* 100083, *China*
[f] *Beijing Research Institute of Uranium Geology, Beijing* 100029, *China*

ARTICLE INFO

Article history:
Received 13 January 2025
Received in revised form 8 April 2025
Accepted 27 April 2025
Available online 28 September 2025

Keywords:
Lishiite
$(Ca_2□)Sr_3(CO_3)_5$
New mineral species
Burbankite group
Carbonatite-syenite complex
Mineral exploration engineering
Shaxiongdong

ABSTRACT

Lishiite, $(Ca_2□)Sr_3(CO_3)_5$, is a new mineral species from Shaxiongdong, Hubei Province, China. It mainly occours as conchoidal crystals and with combination of hexagonal prism and pyramid and is associated with calcite, K-feldspar, albite, aegirine, apatite, and ancylite-(Ce)(?) and strontianite etc. Lishiite is brittle with conchiform fracture and has a Mohs hardness of approximately 4 and none cleavages were observed. The Vickers microhardness (VHN10) is 197.42 kg/mm^2 (range: 166.88 kg/mm^2 to 214.58 kg/mm^2), and the calculated density of lishiite is 3.696 g/cm^3. Hand specimen of lishiite are yellow-brown. The empirical chemical formula of the lishiite is $^{A}(Ca_{1.18}Sr_{0.25}Na_{0.19}□_{1.38})_{\Sigma 3.00}$ $^{B}[Sr_{2.17}(Ce_{0.42}La_{0.24}Nd_{0.09}Eu_{0.01})_{\Sigma 0.76}Ba_{0.07}]_{\Sigma 3.00}$ $(C_{5.05}O_{15})$. As a member of the burbankite group, the general formula of lishiite follows the general formula $A_3B_3(CO_3)_5$, where *A*=Na, Ca, or and *B*=Sr, Ba, *REE*, or Ca. Its crystal structure is hexagonal (space group $P6_3mc$) with unit cell parameters a=10.4898(5) Å, c=6.4167(5) Å, and V=611.47(6) Å^3, characterized by layers of AO_8 and BO_{10} polyhedra connected to $[CO_3]^{3-}$ groups. The discovery of lishiite provides new insights into the evolutionary history of rare earth element (REE) carbonate deposit formation.

1. Introduction

Lishiite (IMA No. 2022–121a), $Ca_2□Sr_3(CO_3)_5$, is a new mineral species form the carbonatite-syenite complex in Shaxiongdong, Hubei, China. Lishiite is named in honour of geologist Li Shi (Chinese name "李石") (1940–2007) who was a senior engineer of the Hubei Geological Testing Center, Wuhan, China for his thorough and effective research on alkaline-carbonatite complexes and their ore-forming processes in western Hubei Province. In addition to lishiite, seven other mineral species share the general formula $A_3B_3(CO_3)_5$, where: A=Na>Ca, REE^{3+}, or vacancies (□); B=Sr, Ca, Ba, REE^{3+}, or Na. These minerals include: burbankite–$(Na,Ca,□)_3(Sr,REE,Ba,Ca)_3(CO_3)_5$, calcioburbankite–$(Na,Ca,REE)_3(Ca,REE,Sr)_3(CO_3)_5$, khanneshite–$(Na,Ca)_3(Ba,Sr,REE,Ca)_3(CO_3)_5$, petersenite-(Ce)–$(Na,Ca)_4(Ce,La,Sr)_2(CO_3)_5$, remondite-(La)–$Na_3(La,Ce,Ca)_3(CO_3)_5$, remondite-(Ce)–$Na_3(Ce,Ca,Na,Sr)_3(CO_3)_5$, and Sanromanite–$(Na_2Ca)Pb_3$. These burbankite-group minerals are typically formed in alkali-carbonate systems and can crystallize over an extremely wide temperature range. (Belovitskaya YV and Pekov V, 2004; Zaitsev AN et al., 1998; Chen TT and Chao GY, 1974). However, they also have been found in alkaline lacustrine depositional system in Eocene Green River Formation, U.S.A. (Fitzpatrick J and Pabst A, 1977) and in host rocks surrounded by the carbonatite complex as fluid inclusions (solid phase) in north-central Namibia (Bernhard B et al., 1999).

In this contribution, we describe the new burbankite group mineral lishiite that was found in Shaxiongdong carbonatite-syenite complexes situated along the southwestern edge of the

First author: *E-mail address*: daijiegirl@163.com (Jie Dai).

* Corresponding author: *E-mail address*: 21958983@qq.com (Xiao-dong Pan).

Literary editor: Xi-jie Chen
doi:10.31035/cg2025163
2096-5192/© 2025 China Geology Editorial Office.

Wudang Terrane–a tectonic unit composed of the Wudang and Yaolinghe groups in the South China Block (Figs. 1b, c). The Wudang and Yaolinghe group rocks have undergone regional greenschist-facies metamorphism.The complexes cut across the Yaolinghe Group strata, exhibiting a predominant ENE-WSW orientation (Fig. 1c). The nepheline-bearing alkali-feldspar syenites contain K-feldspar, albite, and minor biotite, nepheline, muscovite, calcite etc. (Xu C et al., 2008). The carbonatites consist more than 80% calcite and minor K-feldspar, albite, aegirine, biotite, burbankite, apatite, allanite, and pyrite. Burbankite and allanite are the main rare earth minerals in Shaxiongdong carbonatites, and the two minerals account for 1%−2% of the rock's volume (Wang T and Yan FM, 1989). The syenites are intruded by lenticular and vein-like carbonatite dykes, ranging in length from 10 m to 200 m (Fig. 1d).

To study the mineralogical characteristics of lishiite, we collected samples during field geological surveys and conducted comprehensive systematic analyses using optical microscopy, electron probe, X-ray single crystal diffraction, X-ray powder diffraction and other methods. The comprehensive analysis concluded that this mineral is a new species of the burbankite group, making an innovative contribution to the development of new minerals. And the discovery of lishiite provides new insights into the ore-forming processes of REE carbonate deposits, particularly regarding the magmatic fractionation and mineral-paragenetic sequences in carbonatite-syenite complexes.

2. Occurrence

More than 50% of the world's rare earth (REE) deposits are closely related to carbonatites (Weng ZH et al., 2015), such as the famous ultra-large REE deposits: Bayan Obo REE deposit in Inner Mongolia, China (Fan HR et al., 2016), Mao Niuping REE deposit in Sichuan, China (Fu XF et al., 2023; Shen GF et al., 2005), and Mountain Pass REE deposit in California, USA (Watts KE et al., 2022), and about 96% of these deposits are rich in Ce, Y, La, and Nd (Wall F et al., 2017). In addition to rare earth elements (REEs) associated with carbonatites, those related to granites also hold a significant strategic position in China (Guo JC et al., 2024; Cao HW et al., 2022; Zhang M et al., 2018).

Specimens containing lishiite were collected from carbonatite-syenite complexes, located in Zhushan County, about 150 km southwest of the Shiyan city, Hubei Province, China (Fig. 1). Its geographic coordinates are 32° 9′ 14.37″ N and 110° 18′ 46.64″ E. The carbonatites containing lishiite occur mainly as stocks (Fig. 1d, Fig. 2a) associated with syenites. The primary monazite from the carbonatites yields an age of 233.6 ± 1.7 Ma, while the zircon from the syenites yields an age of 766 ± 25 Ma (Xu C et al., 2014).

Associated minerals with lishiite are calcite, K-feldspar,

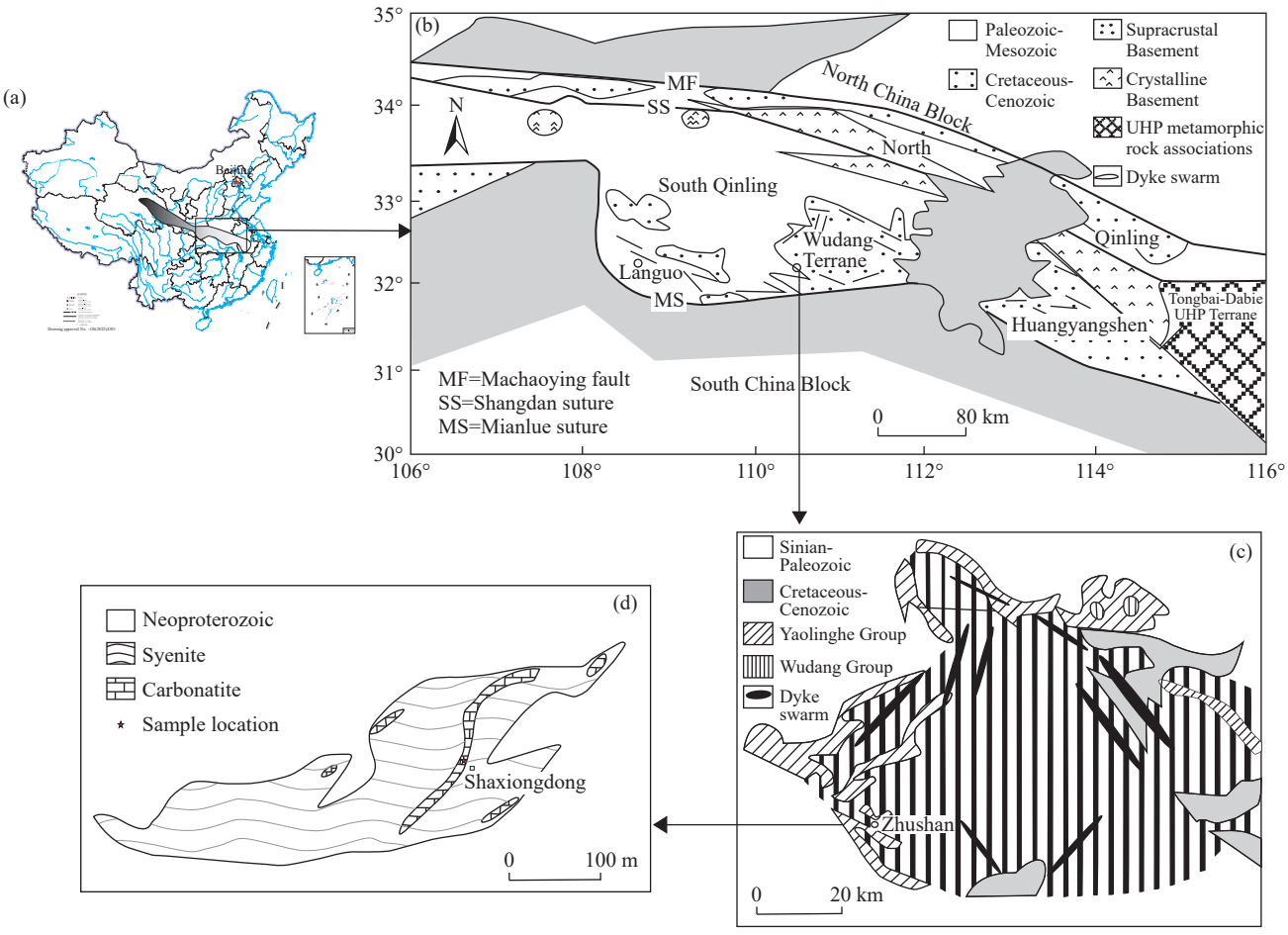

Fig. 1. Geological overview of the Shaxiongdong carbonatites and syenites (modified from Li S, 1991; Xu C et al., 2008).

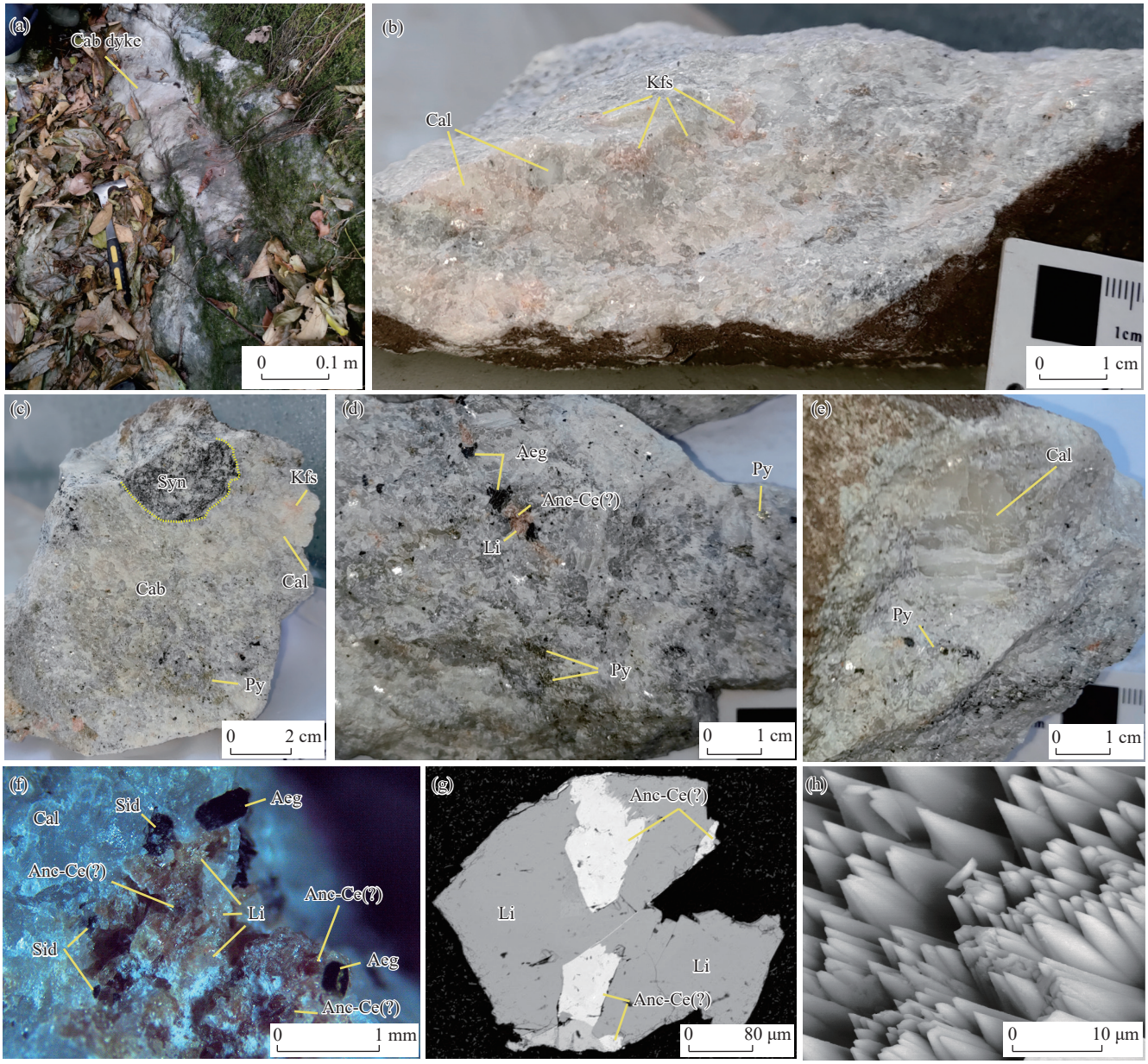

Fig. 2. Photographs showing occurrence of the carbonatites containing lishiite and associated minerals in the carbonatite-syenite complexes. a–carbonatite dyke associated with syenites in the field; b–photo of a hand specimen showing K-feldspar distributed in white carbonatite composed of more than 95% of calcite, with minor K-feldspar; c–carbonatite composed of calcite, minor K-feldspar and pyrite containing syenite xenoliths; d–hand specimen of carbonatite showing lishiite (with yellow brown colour) coexisting with ancylite-(Ce) (?) (with dark brown colour) and aegirine (with black colour); e–photo of a hand specimen showing calcite is more than 1 cm in size, with minor pyrite; f–photo of a hand specimen under binocular microscope showing parageneses of lishiite (yellow brown), calcite (gray-white), siderophyllite (black, clintheriform), aegirine (black, columnar) and ancylite-(Ce) (?) (dark brown), etc.; g–backscattered electron (BSE) image showing close parageneses of lishiite with dark colour and ancylite-(Ce) (?) with light colour; h–backscattered electron image of lishiite with distinct dihexagonal pyramidal habit. Cab–carbonatite; Cal–calcite; Kfs–potash feldspar; Syn–syenite; Py–pyrite; Aeg–aegirine; Anc-Ce–ancylite-(Ce) (?); Li–lishiite; Sid–siderophyllite.

albite, aegirine, siderophyllite, apatite, allanite, pyrite, sphalerite, strontianite and ancylite-(Ce) etc. (Fig. 2b–g). Pyrite occurs as disseminated or granular distribution in carbonatite (Figs. 2c–d). The most closely symbiotic mineral with lishiite is ancylite-(Ce) (?) with dark brown colour under natural light (Fig. 2d) and binocular microscope (Fig. 2f), bright colour while lishiite with dark colour in backscattered electron (BSE) image (Fig. 2g). Under scanning electron microscopy (Fig. 2h), lishiite exhibits a distinct dihexagonal pyramidal habit.

3. Physical and optical properties

Under the SEM, lishiite occurs as euhedral-subhedral crystal ranging from a few tens to hundreds micrometers in size (Fig. 2g). It exhibits a yellow-brown color visible in macroscopic view (Figs. 2b, d, f). No cleavages and parting are observed, and the fracture is conchiform. The new mineral lishiite is brittle and does not exhibit any fluorescence under UV radiation. The streak of lishiite is white, and the luster of lishiite is greasy, and it is non-magnetic. The Vickers

microhardness (VHN, 25 g load) is 197.42 kg/mm^2 (range 166.88−214.58 kg/mm^2), corresponding to a Mohs hardness of approximately 4. The density measured by hydrostatical weighing method is 3.501 g/cm^3, whereas the calculated density is 3.696 g/cm^3 due to the sample being somewhat weathered.

Thermal experiment conducted by JF-A Type Thermal Analyzer indicates that lishiite underwent two decompositions with the evolution of CO_2 (Fig. 3). 50 mg of the sample was used in the experiment under conditions of neutral Body Al and Pt-Rh thermocouple, with a heating rate of 10ºC/min.

Raman spectroscopy of Lishiite was analyzed by Renishaw 2000 Raman Microscope using a 532 nm laser with the power of 40 mW and a spot size of 1 μm. Fig. 4 exhibits Raman shift of lishiite at 2945 cm, 1077 cm, 862 cm, 706 cm, and 277 cm^{-1}, in which bands at 1077 cm, 706 cm, and 277 cm^{-1} are due to the vibrations of $(CO_3)^{2-}$ group. A strong Raman mode at about 1077 cm^{-1} corresponds to the symmetric stretching vibration of the carbonate group. The origin of the bands at 2945 cm, 862 cm, and 277 cm^{-1} requires further investigation.

Lishiite exhibits uniaxial negative optical properties, with a refractive index of ω=1.623, ε=1.612 (at a wavelength of 589 nm). The dispersion is weak, pleochroism is very faint, and in terms of optical properties, the refractive index is along the c-axis direction.

4. Chemical compositions

Lishiite's chemical composition was characterized by using an EPMA-1600 electron microprobe (EMP) at the The Key Laboratory of Sedimentary Basin and Oil and Gas Resources, Ministry of Natural Resources, China, operating in wavelength-dispersive mode with the accelerating voltage of 20 kV, beam current of 10 nA, and a beam diameter of 10 μm. Chemical compositions (in wt %) of lishiite are presented in Table 1. Mg, Sm, and Y are below detection limits. The CO_2 content was determined by wet analysis.

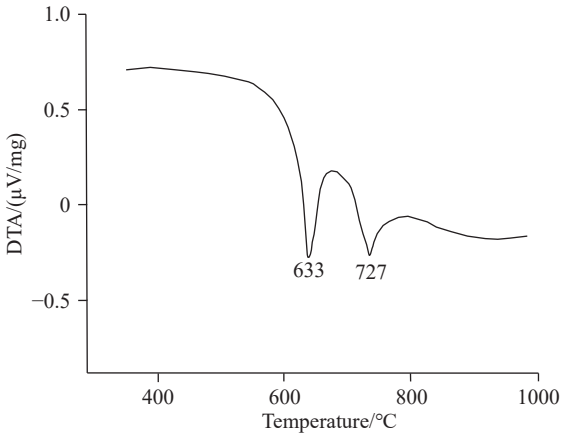

Fig. 3. DTA curve showing thermal behavior of lishiite.

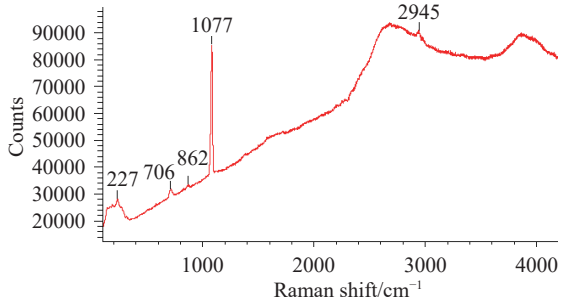

Fig. 4. Raman spectrum of lishiite.

The empirical formula, calculated based on structural refinement O = 15 atoms per formula unit (*apfu*), is $^{A}(Ca_{1.18}Sr_{0.25}Na_{0.19}\square_{1.38})_{\Sigma 3.00}$ $^{B}[Sr_{2.17}(Ce_{0.42}La_{0.24}Nd_{0.09}Eu_{0.01})_{\Sigma 0.76}Ba_{0.07}]_{\Sigma 3.00}$ $(C_{5.05}O_{15})$. The simplified formula is $(Ca,\square,Sr,Na)_3(Sr,Ce,La,Nd,Ba)_3(CO_3)_5$. The ideal formula is $(Ca_2\square)Sr_3(CO_3)_5$. The latter requires SrO 48.34, CaO 17.44, CO_2 34.22; Total 100%.

5. X-ray diffraction and structural refinement

5.1. Crystallography

Single-crystal X-ray diffraction studies were carried out at room temperature (20°C) using a Rigaku XtaLAB PRO-007HF diffractometer equipped with a microfocus rotating-anode MoKα radiation source (λ = 0.71073 Å, 1.2 kW) and a hybrid pixel array detector at the Crystal Structure Laboratory, China University of Geosciences (Beijing). A single-crystal fragment of lishiite with an approximate dimension of 0.010×0.010×0.010 mm was used for the single-crystal XRD experiment. This fragment was extracted by FIB (Focused Ion Beam, Tescan GAIA 3) in Beijing Research Institute of Uranium Geology from the same polished section used for the EMP analysis. The crystal structure determination and refinement were performed using OLEX2-1.3 (Dolomanov OV et al., 2009), with the SHELXT (Sheldrick GM, 2015). The crystal structure data indicate that lishiite has a hexagonal structure, belonging to the space group $P6_3mc$ (#186), with lattice parameters a=10.4898(5) Å, c=6.4167(5) Å, and a unit cell volume of 611.47(6) Å^3 (Z = 2). The a:c ratio calculated from unit-cell parameters is 1.635:1.000.

X-ray powder diffraction data were collected using a Rigaku Oxford Diffraction XtaLAB PRO-007HF, with MoKα radiation at 50 kV and 24 mA, employing the crystal rotation

Table 1. Chemical compositions of lishiite.

Constituent	Mean*	Range	Stand. Dev.	Probe Standard
CaO	9.73	9.89−11.62	0.517	Dolomite
SrO	36.73	34.44−37.89	0.885	Celestine
BaO	1.68	1.64−1.98	0.089	Barite
La_2O_3	5.69	4.84−6.32	0.287	Synth-LaF_3
Ce_2O_3	10.20	9.03−11.79	0.617	Synth-CeF_3
Nd_2O_3	2.20	2.01−2.49	0.156	Synth-NdF_3
Eu_2O_3	0.16	0.11−0.20	0.026	Synth-EuF_3
Na_2O	0.87	0.66−1.32	0.189	Albite
CO_2**	32.58			
Total	99.84			

Notes: *Average of 28 analyses on three crystals, one of them was the structural refinement and X-ray diffraction analysis sample (Fig. 2); ** Wet analysis.

method also in the Laboratory of Crystal Structure, China University of Geosciences (Beijing). Table 2 and Fig. 5 depict the PXRD pattern (MoKα) for lishiite. Powder XRD data refinement yielded the following unit cell dimensions:

Table 2. X-ray powder diffraction data of lishiite.

I_{obs}	I_{calc}	d_{obs}	d_{calc}	h	k	l
92	**14**	**3.4611**	**3.4469**	**1**	**2**	**0**
38	19	3.2162	3.2105	0	0	2
74	**16**	**3.0695**	**3.0399**	**0**	**3**	**0**
20	13	2.7463	2.7475	0	3	1
100	**100**	**2.6147**	**2.6225**	**2**	**2**	**0**
62	11	2.3654	2.3533	1	3	1
48	9	2.2849	2.2799	0	4	0
42	7	2.2150	2.2074	0	3	2
47	45	2.1483	2.1485	0	4	1
35	12	2.0850	2.0837	0	1	3
44	25	2.0451	2.0357	2	2	2
66	**12**	**1.9914**	**1.9901**	**1**	**4**	**0**
63	**24**	**1.9359**	**1.9375**	**0**	**2**	**3**
86	**13**	**1.8577**	**1.8589**	**0**	**4**	**2**
50	11	1.7544	1.7545	0	5	1
71	**17**	**1.6631**	**1.6645**	**2**	**4**	**1**
13	1	1.6094	1.6053	0	0	4
40	5	1.5611	1.5605	0	4	3
47	6	1.5167	1.5185	2	4	2
14	<1	1.4580	1.4574	1	4	3
12	1	1.4144	1.4195	0	3	4
46	6	1.3727	1.3738	0	6	2
36	7	1.3428	1.3424	2	4	3
51	2	1.3132	1.3126	0	4	4
8	<1	1.2822	1.2768	0	7	1
5	1	1.2620	1.2647	2	6	0
28	<1	1.2392	1.2393	0	6	3
23	4	1.2153	1.2179	4	4	2
7	2	1.1770	1.1767	2	6	2
11	<1	1.1432	1.1451	1	3	5
12	3	1.1209	1.1224	0	8	1
17	3	1.1016	1.1037	0	6	4

Crystal system: Hexagonal Space group: $P6_3mc$ (#186)
a = 10.530(5) Å c = 6.4211(10) Å
V = 616.6(7) Å^3 Z = 2

Regarding the powder data, note that since the test sample was cut with Tescan GAIA 3 focused ion beam scanning electron microscope (FIB-SEM) in Beijing Research Institute of Uranium Geology, China, and intercepted from the probe sheet (Fig. 2g) using a nanomanipulator, the sample was only about 10 μm. This leads to the diffraction data were attenuated.

5.2. Crystal structure

The structure refinement using all measured independent data and the reflections with $I > 2\sigma(I)$ resulted in all R factor of 0.0223 (R_1=0.0250 for 586 unique reflections).

The general structural formula of the burbankite-group minerals can be written as $A_3B_3(CO_3)_5$, where A = Na, Ca, or □ and B = Sr, Ba, *REE*, or Ca (Belovitskaya YV et al., 2000).

Similar to the structure of burbankite group minerals, the crystal structure of lishiite contains two independent cationic positions in the center of polyhedrals formed by oxygen atoms and three types of triangular carbonate groups. The eight-vertex polyhedron, AO_8, is occupied predominantly by Ca and a part is vacant according to the composition analysis. The ten-vertex polyhedron, BO_{10}, is occupied predominantly by Sr, *REE* and Ba (with Sr>*REE*>Ba) (Table 3). The polyhedron with 10-coordination is connected at the angular top on the plane (0001) and is connected to the $[CO_3]^{3-}$ arranged parallel to (0001). And 3/5 $[CO_3]^{3-}$ oblique to the c-axis (Wang P et al., 1982).

The crystal structural model of lishiite is shown in Fig. 6. The atomic coordinates and site occupancies for lishiite are shown in Table 4. The anisotropic displacement parameters are given in Table 5. The bond lengths of Ca1 and Sr1 range from 2.3688(16) to 2.716(3) Å and from 2.542(2) to 2.7558(5) Å, respectively, and the selected interatomic distances are illustrated in Table 6. The bond valences are given in Table 7.

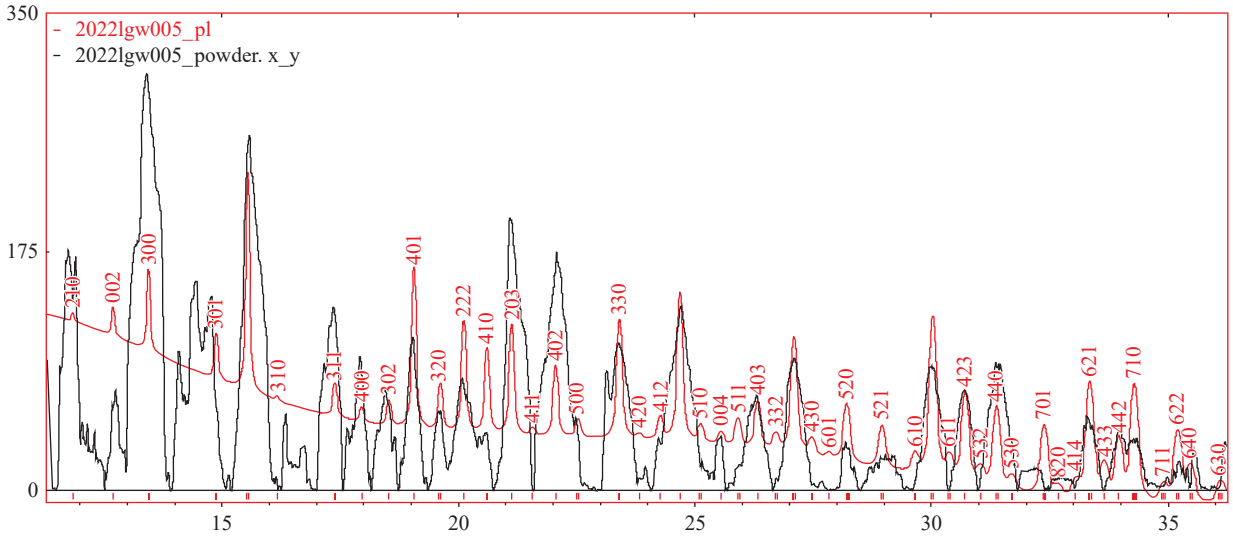

Fig. 5. Comparison of XRPD patterns (MoKα) (black is measured, red is calculated by PowderCell V2.4).

Table 3. Comparison of crystal-chemistry characteristics between lishiite and the known species in burbankite group.

Mineral	Crystal system	Space group	A_3	B_3	$(CO_3)_5$	Ref.
Lishiite	**Hex.**	***P*6$_3$*mc***	**Ca_2□**	**(Sr,REE,Ba)$_3$**	$(CO_3)_5$	This Study
Burbankite	Hex.	*P*6$_3$*mc*	$(Na,Ca)_3$	Sr_3		①
Calcioburbankite	Hex.	*P*6$_3$*mc*	Na_3	$(Ca,Ce,Sr,La)_3$		②
Khanneshite	Hex.	*P*6$_3$*mc*	$(Na,Ca)_3$	$(Ba,Sr,Ce,Ca)_3$		③
Petersenite-(Ce)	Mon.	*P*2$_1$	Na_4	Ce_2		④
Remondite-(Ce)	Mon.	*P*2$_1$	Na_3	$(Ce,Ca,Na)_3$		⑤
Remondite-(La)	Mon.	*P*2$_1$	Na_3	$(La,Ca,Na)_3$		⑥
Sanromanite	Hex.	*P*6$_3$*mc*	Na_2Ca	Pb_3		⑦

Notes: ① Pecora WT and Kerr JH, 1953; ② Van VJ, et al., 1995; ③ Yeremenko GK and Bel'ko VA, 1982; ④ Grice JD et al., 1994; ⑤ Cesbron F et al., 1988; ⑥ Pekov IV et al., 2000; ⑦ Schlter J et al., 2007.

Table 4. Atomic coordinates and site occupancies of lishiite.

Site	Atom	Wyck.	Occ.	*x*	*y*	*z*
A	Ca1	6*c*	0.624(6)	0.52342(10)	0.47658(10)	0.75740(14)
B	Sr1	6*c*	0.957(10)	0.31868(3)	0.159338(17)	1.071008(13)
	Ce1		0.043(10)			
O	O1	6*c*	1.00	0.40397(17)	0.59603(17)	0.5873(7)
	O2	6*c*	1.00	0.4482(4)	0.22411(18)	0.7180(5)
	O3	6*c*	1.00	0.1401(4)	0.07006(18)	0.7347(5)
	O4	12*d*	1.00	0.3733(3)	0.0809(3)	0.4377(4)
C	C1	2*a*	1.00	0	0	0.7360(11)
	C2	6*c*	1.00	0.3985(5)	0.1992(3)	0.5328(7)
	C3	2*b*	1.00	1/3	2/3	0.5823(14)

Table 5. Anisotropic displacement parameters (in Å ^{2}) of lishiite.

	U^{11}	U^{22}	U^{33}	U^{12}	U^{13}	U^{23}
Ca1	0.0186(7)	0.0186(7)	0.0252(11)	0.0076(7)	-0.0002(4)	0.0002(4)
Ce1 Sr1	0.01070(19)	0.00942(16)	0.0102(2)	0.00535(10)	0.0009(3)	0.00045(16)
O1	0.0212(12)	0.0212(12)	0.0182(18)	0.0130(13)	-0.0007(12)	0.0007(12)
O2	0.0151(19)	0.0218(15)	0.0146(17)	0.0075(9)	-0.0038(16)	-0.0019(8)
O3	0.0125(18)	0.0205(16)	0.033(2)	0.0062(9)	-0.0004(18)	-0.0002(9)
O4	0.0168(12)	0.0131(13)	0.0235(14)	0.0058(10)	0.0030(11)	-0.0038(11)
C1	0.014(2)	0.014(2)	0.008(3)	0.0068(12)	0.00000	0.00000
C2	0.008(2)	0.0090(14)	0.011(3)	0.004(1)	0.0034(17)	0.0017(9)
C3	0.014(2)	0.014(2)	0.012(3)	0.0068(10)	0.00000	0.00000

Table 6. Selected bond lengths (Å) of lishiite.

Sr1—O1i	2.7558 (5)	Ca1—O1	2.429 (4)
Sr1—O1ii	2.7558 (5)	Ca1—O2viii	2.3688 (16)
Sr1—O2	2.553 (3)	Ca1—O2	2.3688 (16)
Sr1—O3iii	2.7238 (12)	Ca1—O4iii	2.400 (3)
Sr1—O3	2.700 (3)	Ca1—O4ix	2.400 (3)
Sr1—O3ii	2.7238 (12)	Ca1—O4viii	2.716 (3)
Sr1—O4iii	2.542 (2)	Ca1—O4x	2.716 (3)
Sr1—O4vi	2.648 (3)	**<Ca1—O>**	**2.4947**
Sr1—O4v	2.542 (2)	C1—O3 (×3)	1.273 (3)
Sr1—O4iv	2.648 (3)	C2—O2	1.271 (6)
<Sr1—O>	**2.6592**	C2—O4 (×2)	1.287 (3)
Ca1—O1i	2.494 (4)	C3—O1 (×3)	1.284 (3)

Symmetry codes: (i) 1+y, 1-x+y, 0.5+z; (ii) -y, x-y, z; (iii) x-y, x, 0.5+z; (iv) x, y, 1+z; (v) x-y, -y, 0.5+z; (vi) x, x-y, 1+z; (vii) 1+y, 1-x+y, -0.5+z; (viii) 1-x+y, 1-x, z; (ix) 1-x, 1-x+y, 0.5+z; (x) x, x-y, z; (xi) 1-x, 1-y, 0.5+z; (xii) x-y, x, -0.5+z; (xiii) 1-x, -y, 0.5+z; (xiv) -y, x-y, -1+z; (xv) x, y, -1+z; (xvi) y, -x+y, -0.5+z; (xvii) -x+y, -x, z; (xviii) -x, -y, 0.5+z; (xix) -x+y, 1-x, z.

6. Discussion

6.1. Relation to other species

There were seven named species in the burbankite group before the approval of lishiite. They are burbankite (Pecora WT and Kerr JH, 1953), calcioburbankite (Van VJ et al., 1995), khanneshite (Yeremenko GK and Bel'ko VA, 1982), petersenite-(Ce) (Grice JD et al., 1994), remondite-(Ce) (Cesbron F et al., 1988), remondite-(La) (Pekov IV et al., 2000), and sanromanite (Schlüter J et al., 2007). In the system of Smith and Nickel (2007) and also by checking in the IMA list of unmanned minerals (http://cnmnc.units.it/), a mineral similar to lishiite is not found. According to "The IMA-CNMNC dominant-constituent rule revisited and extended" (Hatert F and Burke EAJ 2008), lishiite can be regarded as a new member of burbankite isotypic series. It is distinguished

Table 7. Bond valences of lishiite.

	B	*A*	C1	C2	C3	Sum
O1	0.181*2+0.008*2 ↓ 0.181+0.008 →	0.149+0.174 ↓→			1.334*3 ↓ 1.334→	1.845
O2	0.276+0.014 ↓→	0.202*2 ↓→		1.378 ↓→		2.072
O3	0.193*2+0.203+0.009*2+0.010 ↓ 0.193+0.203+0.009+0.010 →		1.368*3 ↓ 1.368 →			1.738
O4	0.282*2+0.226*2+0.011*2+0.015*2↓ 0.282+0.226+0.011+0.015 →	0.086*2+0.187*2 ↓ 0.086+0.187 →		1.321*2 ↓ 1.321 →		2.129
Sum	2.355	1.273	4.104	4.020	4.002	

Note: The bond-valence calculations were performed using the equation and constants of Brown ID (1977), $S = \exp[R_0-d_0)/b]$. Bond parameters of Ca^{2+}–O^{2-}, Sr^{2+}–O^{2-}, C^{4+}–O^{2-} are from Gagné OC and Hawthorne FC (2015).

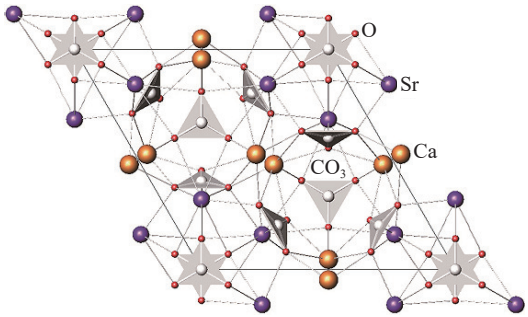

Fig. 6. Crystal structural model of lishiite.

as both Ca-dominant and Sr-dominant at the B site, unlike all previously known members of the burbankite group, in which Na>Ca at the A site (Table 3)

6.2. Ore paragenetic sequence and formation of lishiite

It is suggested that the light rare earth elements (LREEs)-enriched signature of carbonatites reflects the chemistry of their parental magma (Hornig I and Kjarsgaard BA, 1998). Some mantle-derived primary carbonate liquids are rich in REEs, approximately 1000×10^{-6} (Moine BN et al., 2004). The trace element composition of the Shaxiongdong carbonatites indicates enrichment in strontium (Sr) and LREEs, along with negative anomalies in zirconium (Zr)-hafnium (Hf), lead (Pb), scandium (Sc), and chromium (Cr) (Xu C et al., 2010). The chondrite-normalized REE patterns of the carbonatites exhibit a steep negative slope and negligible anomalies for cerium (Ce) and europium (Eu). The strontium (Sr) and neodymium (Nd) isotopic results for the carbonatites and their constituent minerals (calcite, biotite, pyrite, ferrocolumbite, fluorapatite, and monazite) reveal a low level of radiogenic strontium [$(^{87}Sr/^{86}Sr)i \approx 0.7036-0.7040$] and minimal variation in ε_{Nd} values (ranging from +0.6 to −1.1) (Xu C et al., 2010). These isotopic signatures suggest a derivation from an ancient mantle source with minimal crustal contamination. The enriched LREE signatures and specific trace element anomalies observed in the Shaxiongdong carbonatites display distinct differences in terms of their geochemical and mineralogy characteristics.

Rare earth minerals (REE minerals) are important strategic resources. In Shaxiongdong carbonatites, the principal REE minerals are fluorapatite, monazite-(Ce), bastnäsite-(Ce) and synchysite-(Ce). Research indicates that the first two minerals are early phases formed prior to calcite, while the last two minerals crystallized later than the calcite (Xu C et al., 2010). Compared to calcite, these REE minerals are significantly enriched in LREEs.

In most carbonatite systems, late-stage REE fluorocarbonates typically occur with bastnäsite and related minerals in hydrothermal environments (Williams-Jones AE et al., 2000; Samson IM et al., 2004). However, in the Shaxiongdong carbonatites, the REE fluorocarbonates appear to be primary phases rather than products of secondary remobilization and redeposition (Schmitt AK et al., 2002)

Burbankite, the most numerically dominant member of the burbankite group, one of the REE-bearing carbonates (Edahbi M et al., 2018), is often found with burbankite group minerals and alteration products of primary REE-bearing carbonates (Simandl GJ and Paradis S, 2018). Burbankite, together with lishiite is found in Shaxiongdong carbonatite. It has been reported that a burbankite-like structural phase with the composition $Na_2Ca_4(CO_3)_5$ was successfully synthesized at 6 GPa and 1323 K (Rashchenko SV et al., 2017). The environment is located approximately 200 kilometers underground. Additionally, $Na_3Ca_2La(CO_3)_5$ was synthesized at 5 GPa and 1073 K (approximately equivalent to a depth of about 165 kilometers underground) under a Ca-rich alkaline-alkaline earth carbonates environment (Merlini M et al., 2020). These synthetic experiments demonstrate that the incorporation of light REE^{3+} in a burbankite-like structure under the conditions of the upper mantle (Milani S et al., 2022). The geochemical characteristics of carbonatite in Shaxiongdong indicate that their material comes from the upper mantle ($\delta^{18}O$=6.34‰–6.72‰, $\delta^{14}C$=−5.54‰− −5.63‰, $^{87}Sr/^{86}Sr$=0.7032, Li S, 1991). These observations reinforce the link between lishiite and mantle-derived melts.

The primary calcite in the Shaxiongdong carbonatites, which exhibits low REEs contents and flat REE profiles, suggests that REE were fractionated from the parental carbonatite liquid before the precipitation of calcite (Xu C et al., 2010). The P_2O_5 content (0.71%) in primary calcite is significantly lower than the global average for calcite (1.73%) (Le Bas MG, 1981; Wang T and Yan FM, 1989), indicating that the $(PO_4)^{3-}$ ions were initially bound with the abundant Ca^{2+} in the carbonatite liquid, along with substantial F^-, to form fluorapatite. Meanwhile, REE^{3+} could only partially substitute for Ca^{2+} in fluorapatite through polar isomorphism, with a concentration of REE^{3+} being 0.82% (Wang T and Yan

FM, 1989).

The co-occurrence of fluorapatite and monazite-(Ce) indicates that the magma initially possessed high abundances of REEs. The fractional crystallization of these two minerals resulted in the depletion of REEs, particularly LREEs, in the residual liquid (Wyllie PJ et al., 1996; Xu C et al., 2010). However, during this stage, the concentrations of $(CO_3)^{2-}$ and Ca^{2+} remained high in the fluid, along with a substantial amount of Sr^{2+} (host rock SrO=1.89%; Wang T and Yan FM, 1989). Under these conditions, the remaining REE^{3+} could combine with $(CO_3)^{2-}$, Ca^{2+}, and Sr^{2+} to form lishiite, potentially under upper mantle like pressures and temperatures.

7. Conclusions

Lishiite, a new mineral species belonging to the burbankite group with the formula $(Ca_2□)Sr_3(CO_3)_5$, has been discovered in the carbonatite-syenite complex of Shaxiongdong, Hubei Province, China. Named in honor of geologist Li Shi (李石), This mineral exhibits distinct physical and optical properties, including yellow-brown color, conchoidal fracture, Mohs hardness of approximately 4, and uniaxial negative optical character with refractive indices ω=1.623 and ε=1.612. Its crystal structure is hexagonal (space group $P6_3mc$) with unit cell parameters a=10.4898(5) Å, c=6.4167(5) Å, and V=611.47(6) $Å^3$, characterized by layers of AO_8 and BO_{10} polyhedra connected to $[CO_3]^{3-}$ groups.

Chemically, lishiite is distinguished by its Ca-dominant at A site and Sr-dominant at B site, with minor REE (Ce, La, Nd) and Ba, differing from all known burbankite group members that typically have Na>Ca at the A site. The mineral occurs in association with calcite, K-feldspar, aegirine, apatite, monazite-(Ce), and ancylite-(Ce), reflecting its formation in an alkaline-carbonatite magmatic system.

The genesis of lishiite is closely tied to the magmatic evolution of REE-enriched carbonatites. Early-stage fractional crystallization of fluorapatite and monazite-(Ce) led to REE depletion, particularly of LREEs, in the residual melt, while Ca^{2+}, Sr^{2+}, and $(CO_3)^{2-}$ remained in high concentrations. Lishiite subsequently formed as a primary phase under upper-mantle like pressure temperature conditions, co-precipitating with late-stage REE minerals such as burbankite and bastnäsite-(Ce) from the REE-bearing residual melt. This process underscores the critical role of cation availability and physicochemical conditions in stabilizing burbankite-group minerals.

Lishiite expands the diversity of the burbankite group and provides new insights into the ore-forming processes of REE carbonate deposits, particularly the magmatic fractionation and mineral-paragenetic sequences in carbonatite-syenite complexes.

CRediT authorship contribution statement

Jie Dai and Gan-fu Shen conceived of the presented idea. Guo-wu Li did X-ray diffraction experiment and structural refinement. Guan Wang, Jin-sha Xu, and Kun-yang Wang carried out the EPMA experiment. Jia-le He and Jing Ren did Laser Raman Spectrum experiment. Shang-ke Xie worked for field work. Tao Wang and Ting Li cut samples using FIB-SEM. Jie Dai, Gan-fu Shen, Xiao-dong Pan and Guo-wu Li mainly contributed to the final manuscript. All authors discussed the results.

Declaration of competing interest

The authors declare no conflicts of interest.

Acknowledgments

The authors are grateful to Chuan-long Mou for his help and the professional advice, to Qi Deng for his foundation supporting the field work. The authors sincerely appreciate the constructive suggestions from three anonymous peer reviewers and Editorial Board of China Geology. This research was jointly supported by the project China Geological Survey (DD202501026090) and the National Key Research and Development Program of China (2024YFC2910102).

Supplementary attachment

Supplementary attachment of the acceptance letter from Ferdinando Bosi, Chairman of the CNMNC (Commission on New Minerals, Nomenclature and Classification of the International Mineralogical Association) and the lishiite.cif document to this article can be found online at doi: 10.31035/cg2025163.

References

Belovitskaya YV, Pekov IV, Kabalov YK. 2000. Refinement of the crystal structures of low-rare-earth and “typical” burbankites by the Rietveld method. Crystallography Reports, 45(1),26–29. doi: 10.1134/1.171131.

Belovitskaya YV and Pekov V. 2004. Genetic mineralogy of the burbankite group. New Data on Minerals, 39, 50–64. https://rruff.info/uploads/NDMM39_50.pdf.

Brown ID. 1977. Predicting bond lengths in inorganic crystals. Acta Crystallographica Section B Structural Crystallography and Crystal Chemistry, 33(5), 1305–1310. doi: 10.1107/s0567740877005998.

Bernhard B, Andrew HR, Martin R, Martin H, and Arndt K. 1999. Burbankite, a (Sr, REE, Na, Ca)-carbonate in fluid inclusions from carbonatite-derived fluids: Identification and characterization using Laser Raman spectroscopy, SEM-EDX, and synchrotron micro-XRF analysis. American Mineralogist, 84(7–8), 1117–1125. doi: 10.2138/am-1999-7-814.

Cao HW, Li GM, Zhang LK, Zhang XF, Yu X, Chen Y, Lin B, Pei QM, Tang Li, Zou H. 2022. Genesis of Himalayan leucogranite and its potentiality of rare-metal mineralization. Sedimentary Geology and Tethyan Geology, 42(2), 189–211 (in Chinese with English abstract). doi: 10.19826/j.cnki.1009-3850.2022.04004.

Cesbron F, Gilles C, Pelisson P and Saugues JC. 1988. La rémondite (Ce), un nouveau carbonate de terres rares de la famille de la burbankite. Comptes Rendu, Academie des Sciences, Paris, Ser II, 307, 915–920 (in French with English abstract).

Chen TT, Chao GY. 1974. Burbankite from Mont St. Hilaire, Quebec. Canadian Mineralogist, 12, 342–345.

Dolomanov OV, Bourhis LJ, Gildea RJ, Howard JAK, Puschmann H. 2009. OLEX2: A complete structure solution, refinement and analysis program. Journal of Applied Crystallography, 42(2), 339–341. doi: 10.1107/s0021889808042726.

Edahbi M, Plante B, Benzaazoua M, Kormos L, Pelletier M. 2018. Rare earth elements (La, Ce, Pr, Nd, and Sm) from a carbonatite deposit: Mineralogical characterization and geochemical behavior. Minerals, 8(2), 55. doi: 10.3390/min8020055.

Fan HR, Yang KF, Hu FF, Liu S, Wang KY. 2016. The giant Bayan Obo REE-Nb-Fe deposit, China: Controversy and ore genesis. Geoscience Frontiers, 7(3), 335–344. doi: 10.1016/j.gsf.2015.11.005.

Fitzpatrick J, Pabst A. 1977. Burbankite from the Green River Formation, Wyoming. American Mineralogy, 62 (1–2), 158–163.

Fu XF, Hao XF, Ruan LS, Liang B, Zhang GQ, Hou LW, Pan M, Tang Y. 2023. Metallogenic characteristics and exploration prospecting of the 3R mineral resources in Sichuan, China. Sedimentary Geology and Tethyan Geology, 43(1), 1–18 (in Chinese with English abstract). doi: 10.19826/j.cnki.1009-3850.2022.05006.

Gagné OC, Hawthorne FC. 2015. Comprehensive derivation of bond-valence parameters for ion pairs involving oxygen. Acta Crystallographica Section B, Structural Science, Crystal Engineering and Materials, 71(5), 562–578. doi: 10.1107/S2052520615016297.

Guo JC, Nie F, Wu SY, Liu H, Zou JZ, Ran GH, Lei D, Lai YG. 2024. The discovery and geological significance of the Mantoushan ion-adsorption type heavy rare earth deposit in Dechang, western Sichuan. Sedimentary Geology and Tethyan Geology, 44(1), 86–99 (in Chinese with English abstract). doi: 10.19826/j.cnki.1009-3850.2023.10004.

Grice JD, Van Velthuizen J, Gault RA. 1994. Petersenite-(Ce), a new mineral from Mont Saint-Hilaire, and its structural relationship to other REE carbonates. The Canadian Mineralogist, 32, 405–414.

Hatert F, Burke EAJ. 2008. The ima-cnmnc dominant-constituent rule revisited and extended. The Canadian Mineralogist, 46(3), 717–728. doi: 10.3749/canmin.46.3.717.

Hornig I, Kjarsgaard BA. 1998. Chemistry of perovskite from kimberlites and mantle xenoliths: Implications for the trace element chemistry of the mantle. Extended Abstracts of the 7th International Kimberlite Conference, Cape Town, 331–333.

Le Bas MJ. 1981. Carbonatite magmas. Mineralogical Magazine, 44(334), 133–140. doi: 10.1180/minmag.1981.044.334.02.

Li S, 1991. Geochemistry and petrogenesis of the Shaxiongdong carbonatites, Hubei Province. Geochimica 3, 245–254 (in Chinese with English abstract).

Merlini M, Milani S, Maurice J. 2020. Structures and crystal chemistry of carbonate at Earth's mantle conditions. Carbon in Earth's Interior, edited by: Manning C, Lin JF, Mao W, Geophysical Monograph Series, AGU, John Wiley and Sons, 87–95. doi: 10.1002/9781119508229.ch9.

Milani S, Spartà D, Fumagalli P, Joseph B, Borghes R, Chenda V, Maurice J, Bais G, Merlini M. 2022. High-pressure and high-temperature structure and equation of state of $Na_3Ca_2La(CO_3)_5$ burbankite, European Journal of Mineralogy, 34, 351–358, doi: 10.5194/ejm-34-351-2022.

Moine BN, Grégoire M, O'Reilly SY, Delpech G, Sheppard SMF, Lorand JP, Renac C, Giret A, Cottin JY. 2004. Carbonatite melt in oceanic upper mantle beneath the Kerguelen Archipelago. Lithos, 75(1–2), 239–252. doi: 10.1016/j.lithos.2003.12.019.

Pecora WT, Kerr JH. 1953. Burbankite and calkinsite, two new carbonate minerals from Montana. American Mineralogist, 38, 1169–1183. http://www.minsocam.org/ammin/AM38/AM38_1169.pdf.

Rashchenko SV, Bakakin VV, Shatskiy AF, Gavryushkin PN, Seryotkin YV, Litasov KD. 2017. Noncentrosymmetric $Na_2Ca_4(CO_3)_5$ carbonate of "$M1_3M2_3XY_3Z$" structural type and affinity between borate and carbonate structures for design of new optical materials. Crystal Growth & Design, 17(11), 6079–6084. doi: 10.1021/acs.cgd.7b01161.

Samson IM, Wood SA, Finucane K. 2004. Fluid inclusion characteristics and genesis of the fluorite-parisite mineralization in the snowbird deposit, Montana. Economic Geology, 99(8): 1727–1744. doi: 10.2113/gsecongeo.99.8.1727.

Schmitt AK, Trumbull RB, Dulski P, Emmermann R. 2002. Zr-Nb-REE mineralization in peralkaline granites from the Amis complex, brandberg (Namibia): Evidence for magmatic pre-enrichment from melt inclusions. Economic Geology, 97(2): 399–413. doi: 10.2113/gsecongeo.97.2.399.

Schlüter J, Malcherek T, Pohl D. 2007. Sanromanite, $Na_2CaPb_3(CO_3)_5$, from the Santa Rosa mine, Atacama desert, Chile, a new mineral of the burbankite group. Neues Jahrbuch Für Mineralogie-Abhandlungen, 183(2), 117–121. doi: 10.1127/0077-7757/2007/0068.

Sheldrick GM. 2015. SHELXT-integrated space-group and crystal-structure determination. Acta Crystallographica Section A, Foundations and Advances, 71 (1), 3–8. doi: 10.1107/S2053273314026370.

Shen GF, Yang GM, Xu JS. 2005. Maoniupingite-Ce: A new rare-earth mineral from the Maoniuping rare-earth deposit in Mianning, Sichuan. Sedimentary Geology and Tethyan Geology, 25(1–2), 210–216 (in Chinese with English abstract).

Simandl GJ, Paradis S. 2018. Carbonatites: Related ore deposits, resources, footprint, and exploration methods. Applied Earth Science, 127(4), 123–152. doi: 10.1080/25726838.2018.1516935.

Smith DGW, Nickel EH. 2007. A system for codification for unnamed minerals: Report of the Subcommittee for Unnamed Minerals of the IMA Commission on New Minerals, Nomenclature and Classification. Canadian Mineralogist, 45, 983–990 doi: 10.2113/gscanmin.45.4.983.

Van Velthuizen J, Gault R, Grice JD. 1995. Calcioburbankite, $Na_3(Ca, REE, Sr)_3(CO_3)_5$, a new mineral species from Mont Saint Hilaire, Quebec, and its relationship to the burbankite group of minerals. The Canadaian Mineralogist, 33, 1231–1235.

Weng ZH, Jowitt SM, Mudd GM, Haque N. 2015. A detailed assessment of global rare earth element resources: Opportunities and challenges. Economic Geology, 110(8), 1925–1952. doi: 10.2113/econgeo.110.8.1925.

Watts KE, Haxel GB, Miller DM. 2022. Temporal and petrogenetic links between Mesoproterozoic alkaline and carbonatite magmas at mountain pass, California. Economic Geology, 117(1), 1–23. doi: 10.5382/econgeo.4848.

Wall F, Rollat A, Pell RS. 2017. Responsible sourcing of critical metals. Elements, 13(5), 313–318. doi: 10.2138/gselements.13.5.313.

Pekov IV, Chukanov NV, Kononkova NN, Zadov AE, Belovitskaya YV. 2000. Remondite-(La) $Na_3(La, Ce, Ca)_3(CO_3)_5$–a new mineral of the burbankite family. Zapiski Vserossiyskogo Mineralogicheskogo Obshchestva, 129, 53–60 (in Russian with English abstract).

Wang P, Pan ZL, Weng LB. 1982. Systematic Mineralogy (Volume Ⅲ). Beijing, Geological Press, 375–376 (in Chinese).

Wang T, Yan FM. 1989. Burbankite in Biotite-Aegirine Carbonatite from Hubei Province. Acta Mineralogica Sinica, 9(4), 345–351 (in Chinese).

Wyllie PJ, Jones, AP, Deng J. 1996. Rare earth elements in carbonate-rich melts from mantel to crust. In: Jones AP, Wall F, Williams CT (Eds.), Rare Earth Minerals: Chemistry, Origin and Ore Deposits. The Mineralogical Society Series, Chapman and Hall, London, 7, 77–103.

Williams-Jones AE, Samson IM, Olivo GR. 2000. The genesis of hydrothermal fluorite-REE deposits in the gallinas mountains, new Mexico. Economic Geology, 95(2), 327–341. doi: 10.2113/gsecongeo.95.2.327.

Xu C, Campbell IH, Allen CM, Chen YJ, Huang ZL, Qi L, Zhang GS, Yan ZF. 2008. U-Pb zircon age, geochemical and isotopic characteristics of carbonatite and syenite complexes from the Shaxiongdong, China. Lithos, 105(1–2), 118–128. doi: 10.1016/j.lithos.2008.03.002.

Xu C, Chakhmouradian AR, Taylor RN, Kynicky J, Li WB, Song WL, Fletcher IR. 2014. Origin of carbonatites in the south Qinling Orogen: Implications for crustal recycling and timing of collision between the south and North China blocks. Geochimica et Cosmochimica Acta, 143, 189–206. doi: 10.1016/j.gca.2014.03.041.

Xu C, Kynicky J, Chakhmouradian AR, Campbell IH, Allen CM. 2010. Trace-element modeling of the magmatic evolution of rare-earth-rich carbonatite from the Miaoya deposit, Central China. Lithos, 118(1–2), 145–155. doi: 10.1016/j.lithos.2010.04.003.

Yeremenko GK, Bel'ko VA. 1982. Khanneshite, (Na, Ca)3(Ba, Sr, RE, $Ca)_3(CO_3)_5$–a new mineral of the burbankite group. Zapiski Vserossiyskogo Mineralogicheskogo Obshchestva, 111, 321–324 (in Russian).

Zaitsev AN, Wall F, Le Bas MJ. 1998. REE-Sr-Ba minerals from the khibina carbonatites, Kola Peninsula, Russia: Their mineralogy, paragenesis and evolution. Mineralogical Magazine, 62(2), 225–250. doi: 10.1180/002646198547594.

Zhang M, Li Y, He XC, Feng JL, Zheng Y, Wang HK, Du JG, Wang SS. 2018. Mineralization of the ion adsorption-type REE deposits in the central part of the Lincang granites in western Yunnan. Sedimentary Geology and Tethyan Geology, 38(4), 37–47 (in Chinese with English abstract).